Velocity analysis of vertical seismic profile (VSP) survey at JAPEX/JNOC/GSC Mallik 2L-38 gas hydrate research well, and related problems for estimating gas hydrate concentration

A. Sakai[1]

Sakai, A., 1999: Velocity analysis of vertical seismic profile (VSP) survey at JAPEX/JNOC/GSC Mallik 2L-38 gas hydrate research well, and related problems for estimating gas hydrate concentration; in *Scientific Results from JAPEX/JNOC/GSC Mallik 2L-38 Gas Hydrate Research Well, Mackenzie Delta, Northwest Territories, Canada, (ed.) S.R. Dallimore, T. Uchida, and T.S. Collett; Geological Survey of Canada, Bulletin 544, p. 323–340.*

Abstract: A VSP survey was conducted at the JAPEX/JNOC/GSC Mallik 2L-38 gas hydrate research well to determine elastic-wave velocities that were estimated by traveltime inversion of zero-offset VSP and wavefield inversion of offset VSP data. Shear-wave velocity is estimated to be slower from VSP data than from wireline DSI measurements in the depth interval from 677 m to 889 m. The compressional-wave velocity difference between the VSP- and DSI-derived velocities are comparatively small. Synthetic seismograms from the drift-corrected DSI velocity log correlate well with VSP sections, especially for compressional waves. Azimuthal anisotropy is suggested in VSP shear-source data and the mode of anisotropy appears to change around the base of permafrost.

By comparing computed elastic velocities with drift-corrected DSI velocity logs, two opposing gas hydrate saturation models are examined. Shear wave velocity proved to be the key data to select the correct model. The observed elastic velocity fits the computed elastic velocity for the model of gas hydrate disseminated in pore-space with little cementation at the grain boundaries.

Résumé : Un profilage sismique vertical (PSV) a été effectué au puits de recherche sur les hydrates de gaz JAPEX/JNOC/GSC Mallik 2L-38 afin de déterminer la vitesse des ondes élastiques qui avait été estimée par le traitement de données (inversion des temps de parcours des ondes de PSV à source non déportée et inversion des champs d'ondes de PSV à source déportée). Dans l'intervalle de profondeur de 677 à 889 m, la vitesse des ondes de cisaillement estimée à partir des données de PSV est moins élevée que la vitesse mesurée lors de diagraphies de puits effectuées au moyen d'un imageur sonique dipolaire. La différence dans la vitesse des ondes de compression dérivée à partir des données de PSV et des données provenant de l'imageur sonique dipolaire est relativement faible. Des sismogrammes synthétiques élaborés à l'aide de diagraphies soniques à décalage corrigé sont en bonne corrélation avec les sections de PSV, notamment pour ce qui est des ondes de compression. Les données de PSV avec source d'ondes de cisaillement suggèrent une anisotropie azimutale et le mode d'anisotropie semble changer à proximité de la base du pergélisol.

En établissant une comparaison entre les vitesses calculées des ondes élastiques et les diagraphies soniques à décalage corrigé, nous examinons deux modèles divergents de la saturation en hydrates de gaz. La vitesse des ondes de cisaillement se révèle être la donnée clé pour choisir le modèle correct. La vitesse observée des ondes élastiques correspond à la vitesse calculée pour le modèle des hydrates de gaz disséminés dans les espaces poraux avec peu de ciment aux limites des grains.

[1] Japan Petroleum Exploration Company, Ltd. (JAPEX), 2-2-20 Higashi-shinagawa, Shinagawa-ku, Tokyo 140-0002, Japan

INTRODUCTION

In the Mackenzie Delta of northern Canada, during the period from February to March 1998, the arctic gas hydrate research well JAPEX/JNOC/GSC Mallik 2L-38 was successfully drilled. A significant amount of gas-hydrate-bearing core was recovered, and showed more than 70% pore saturation within the 886–952 m depth range. The Mallik 2L-38 vertical seismic profiling (VSP) and conventional wireline survey were conducted as an experiment on a permafrost-related gas hydrate accumulation.

Major objectives related to the Mallik 2L-38 VSP survey were the evaluation of gas hydrate saturation using compressional- and shear-wave velocity data from VSP and conventional logging data, and the spatial imaging of major gas-hydrate-related seismic features combined with the inversion analysis of the surface seismic data. The Mallik 2L-38 VSP survey consisted of two different source modes (horizontally and vertically directed source motion), and a zero-offset and a single offset point. The vertically directed source mode was used to estimate the spatial velocity structure and to image subsurface reflectors.

On land, the shear-wave velocity can be calculated on the basis of the shear-wave source and receiver pairs used. This is in contrast to marine surveys, where shear-wave velocity can be estimated by the analysis of the converted shear wave only for the compressional-source survey. Prior to this study, no reliable shear-wave surveys had been conducted for the purpose of gas hydrate quantification.

Two opposing gas hydrate reservoir models are proposed based on elastic grain aggregates (Sakai, 1997). One of the models is tentatively called the 'compaction model' in which the gas hydrate is disseminated in the sediment pore space. The increase of the gas hydrate in pore space is believed to have a weak effect on the shear-wave velocity, while the compressional-wave velocity is simulated by the normally compacted sediment. The other model is the 'cementation model' in which the sediment framework (matrix) is stiffened by increasing the gas hydrate, which acts as a cementing agent at the grain boundaries. The increase in gas hydrate in the sediment is believed to have significant effects on the shear-wave velocity as well as compressional-wave velocity. These models were examined using reliable compressional- and shear-wave velocity data. In the computations of the elastic velocity in the gas-hydrate-bearing layers, the dissemination or compaction model closely simulates the calibrated elastic velocities. The model matches well with the field observations of the recovered cores by on-site scientists and is demonstrated quantitatively in the seismic frequency scale from the geophysical data.

DATA ACQUISITION AND SURVEY SPECIFICATIONS

A VSP survey was conducted during the period from March 24 through 25, 1998, by using two IVI Mini Vibrators with Schlumberger CSI™ (combinable seismic imager) three-component receiver cable.

For the zero-offset VSP survey, one vibrator was used for the vertical-source motion and the other vibrator was for the horizontal-source motion in the well. For the zero-offset-source VSP at 33.9 m from the well head, the receiver-level intervals in the depth range between 1145 and 500 m were 5 m and 15 m for the vertical- and horizontal-source motions, respectively. At a point 400.7 m from the well head, two vibrators were used as a vertical-source motion which was recorded in the well at 5 m intervals in the depth range between 1145 and 240 m. The location data for the well and VSP source positions are summarized in Table 1 and the schematic map of the survey area is illustrated in Figure 1. All depths were measured from kelly bushing (KB): 8.31 m above sea level. The depth data for the final processed sections were reduced to the mean sea level unless noted otherwise.

A vibrating source was swept for 12 s with 0.2 s taper at both ends of the 3 s sweep listening time. Sweep-frequency bands for the zero-offset VSP were 10–200 Hz for vertical-source motion, and 50–10 Hz for horizontal-source motion. For the offset-source VSP, a sweep frequency ranging from 10–100 Hz was used. The sweep controller was a Pelton ESG/mini version 6 and every sweep was monitored during the survey. According to the statistical analysis of all the sweeps, the operation was conducted at the higher performance level. The VSP data were recorded at 1 ms sampling intervals with a 300 Hz low pass filter using a Schlumberger Maxis500™ system. Survey specifications are summarized in Table 2.

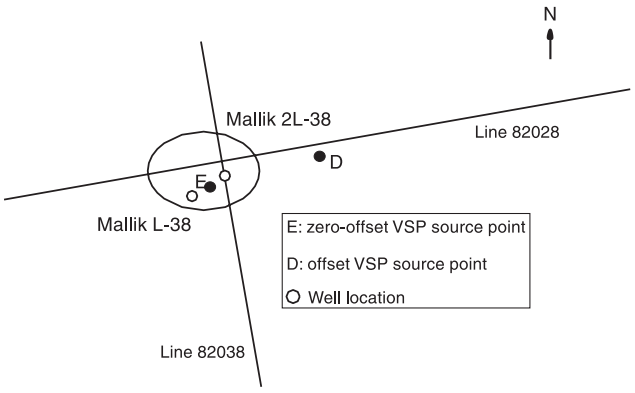

Figure 1. *Schematic map of the survey area, showing the position of the Mallik L-38 and Mallik 2L-38 wells, sources of zero-offset and offset VSPs, and seismic lines 82028 and 82038.*

For the shear-wave source mode, the sweep frequency to band was reduced to 50 Hz to strengthen the effective source energy. The deterioration of higher energy frequencies was related to the bad coupling of the horizontal source on the ground. The VSP survey was conducted without any disruptions in the wireline. Some of the generators at the rig camp were shut down during the survey and the ambient noises made by the generators were not serious, but noises generated by strong wind at the rig site appear to have caused lower frequency noises on the seismic records. Tool coupling in the open-hole interval below 676 m was accurately predicted, measured, and simultaneously monitored using caliper and GR logs.

Data quality degraded above a depth of approximately 250 m in the cased-hole zone. This was due to severe caving of the hole and poor coupling between the casing and the borehole. The first-arrival seismic waves at the shallower levels for the offset-VSP survey were weak. The first arrivals reach the receivers in diffracted waves as the velocity decreases in the permafrost zone. Direct shear waves showed stronger vertical amplitudes at depths less than approximately 400 m.

Table 1. Location data for the Mallik 2L-38 well and VSP source positions.

	Latitude (N)	Longitude (W)	Elevation (m)
Mallik 2L-38	69°27′40.71″	134°39′30.37″	1.15
zero-offset	69°27′44.27″	134°38′54.95″	1.20
offset	69°27′39.70″	134°39′31.58″	1.15

Table 2. Specifications for the VSP survey.

Source of VSP: IVI MiniVibrator	
two for offset VSP one for zero-offset VSP of compressional and shear mode respectively	
Levels of zero offset VSP:	
depth interval receiver interval	500–1145 m 5 m for compressional source 15 m for shear source
Levels of offset VSP:	
depth interval receiver interval	240–1145 m 5 m for compressional source
Sweep:	
linear sweep sweep time listen time sampling rate	 12 sec 3 sec 1 msec
Sweep frequency bands:	
zero offset compressional source zero offset shear source offset compressional source	10–200 Hz 10–50 Hz 10–100 Hz
Receiver:	
Schlumberger CSI	

Other VSP survey types are available (e.g. walkaway VSP), but the ground and weather conditions made these options unfeasible at Mallik 2L-38. There would have been no way to ensure the source couplings were made at each vibrating point within the strict time constraints that were imposed on the rig.

SLOWNESS DATA FROM LOGGING DATA

Corrections of raw slowness data

As discussed in Sakai (1998), the first estimate of compressional- and shear-wave velocities derived by downhole DSI (dipole sonic imager) measurements were degraded as they were partly contaminated by picking stronger amplitude waves transmitted in the well casing. Due to severe borehole problems during the first run in the permafrost zone, the second run of the wireline survey, including the DSI measurement, was operated in the cased hole above 676 m to fill in the missing recording interval at the bottom of the first run.

Compressional-wave slowness or transit time was computed from MPS (monopole P&S mode) waveforms and the shear-wave slowness was estimated from UPS (upper dipole mode) dispersive flexural waveforms recorded by the DSI tool. Originally processed logging data showed slowness-data fluctuations, especially in the cased-hole interval as the slowness-time-coherence (STC) processing was not done properly for weak first arrivals and wrongly picked faster waves transmitted in the casing. The STC processing was based on semblance computations for the slowness-versus-arrival-time diagram using eight measured waveforms which were spaced at 6 inch intervals and spanned 3.5 feet, thus limiting the depth resolution. The flexural-mode slowness is a simple function of frequency and becomes greater than the shear-wave transit-time log at a higher frequency where the formation shear-wave velocity is slower than the borehole fluid velocity (Kurkjian and Chang, 1986; Chen, 1988; Schmitt, 1988). At lower frequency, the dipole source is replaced by a simple shear-wave source and the borehole effects can be reduced. As frequency increases, the resultant energy is more concentrated near the borehole and flexural-mode wavetrains prevail (Kurkjian, 1986, Randall et al., 1991). Low-pass filtering and slowness-bias correction from the transition frequency of the flexural-wave dispersion relation are necessary to estimate the exact formation shear-wave velocity. Slowness bias is a function of source waveform, borehole radius, and borehole fluid and formation slowness and density. The formation shear slowness and borehole radius are significant parameters in determining the slowness bias. There are several borehole conditions of concern such as mudcake, casing, free pipe without complete cementing, borehole washout, invasions, inhomogeneity of the borehole wall, and anisotropy (Everhart and Chang, 1985). Bias correction may exceed 10% of the actual formation shear-wave velocity. In this case, data in both cased and open-hole interval were re-evaluated.

Traveltimes calculated from VSP data are free from the existence of casing effects and several adverse borehole effects, if the cement behind the casing is sufficient and the receiver-tool coupling is suitable. Depth-versus-one-way-traveltime curves derived from the VSP data are used for the calibration of the compressional- and shear-wave slowness or transit-time log data.

VSP DATA PROCESSING

The three-component VSP data provide the compressional- and shear-wave velocities and a high-resolution reflection image around the well site.

Wavefield separation

Zero-offset compressional-source-mode VSP

For zero-offset VSP with a compressional-source mode, after vibrating records are edited and common-receiver data are stacked, upcoming and downgoing compressional waves are separated and the upcoming wavefield is deconvolved by zero-phase deconvolution determined from the downgoing wavefield. Multiple events in the downgoing wavefield are not clear, and the deconvolution has the effect of the shaping in the frequency bands. The compressional-wave velocity structures are estimated and zero-offset reflection sections are computed in the course of processing.

Zero-offset shear-source-mode VSP

For zero-offset VSP with a shear-source mode, the processing scheme is essentially the same as for the compressional-source mode, except for the reorientation of the horizontal components. Recorded horizontal components (X and Y) are transformed into radial and transverse components using particle-motion analyses based on the covariance method. Tool orientations are not independently measured for horizontal components, and compressional-wave motions at the receivers are close to being vertical, as the offset distance is very small. The vibrator motion is set perpendicular to the direction of the source to the well, such that the transverse motion of the observed records is presumably assigned in the same direction as the stronger amplitude motion. After separating the horizontal motions into both radial and transverse motions, the birefringence between the two motions is observed and will be discussed in the following section.

Offset compressional-source-mode VSP

For offset VSP with a compressional-source mode, the processing is performed in the following way. After editing records and stacking common receiver data, the horizontal components are reoriented into radial and transverse components using the polarization data of the first compressional wave motion. It is assumed that the subsurface structure is two dimensional in cross-section and has no structural change in the perpendicular direction, which is primarily justified by the existing surface seismic-survey data. The reorientation of the horizontal components is straightforward using the compressional-wave polarization analysis. Three methods for separating compressional and shear wavefields were examined (Devaney and Oristaglio, 1986; Dankbaar, 1987). The first method uses the wavenumber-frequency domain, and the second method uses the space-frequency domain. The first method assumes a locally homogeneous medium in the depth range spanning several receivers for the analysis in the wavenumber domain, while the second one depends less on the homogeneity of the medium. The last method is a model-based approach starting from the known compressional- and shear-wave velocity field that is constrained by conventional wireline data. In order to evaluate a finer velocity structure in the Mallik 2L-38 well, the inversion based on the first method was applied for the estimation of the velocity structure, incident angles to the receivers, and linearly superimposed wavefields. The inversion methods applied were the 'blind estimate' of the velocity structures, and the resolution problem in the seismic methods was examined.

Velocity analysis

First-break picking for zero-offset VSPs

The compressional-wave and shear-wave velocity fields can be primarily determined by the apparent traveltime of the first-break reading at densely spaced receiver levels. These traveltime values are compared with the integrated sonic transit-time data derived from DSI measurements of the monopole source for compressional waves and the dipole source for shear waves. They can be used to calibrate the traveltime discrepancy caused by tool malfunctioning, poor borehole conditions for wireline data, the nature of the analyzed wavetrain such as dispersive waves, and other problems.

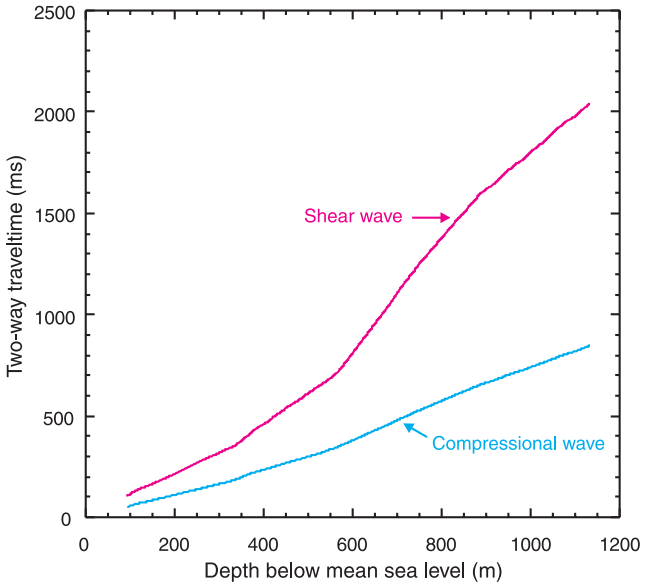

Figure 2. *Relationship between vertical two-way traveltime and depth for compressional and shear waves.*

The first breaks, corresponding to peaks or troughs, were affected by signal-to-noise ratio in the neighbourhood of the picking time, and then the statistical picking method which is based on an AIC (Akaike's Information Criterion) for AR (autoregression) model of one-dimensional travelling waves was examined. Readings resulting from both methods were compared (Tjostheim, 1975; Yokota et al., 1981). If poor quality data are rejected, readings of the first breaks by both methods were essentially the same and it was difficult to determine the first breaks in such poor-quality data by either method. The depth-versus-two-way-traveltime curves are illustrated for compressional and shear waves in Figure 2.

Parametric inversion method for offset VSP

The velocity data were estimated for offset VSP by the inversion method independently from the traveltime picking of the first breaks of zero-offset VSPs. The governing equation is given below (Leaney, 1990). A horizontally stratified medium is assumed over receivers for the purposes of calculation. At a given depth level z, the array of a three-component data with N neighbouring depth levels is modelled as the linear superimposition of elastic waves with locally planar waveforms in a formula that extends components of 1, 2, and N as follows:

$$\begin{pmatrix} \hat{u}_1(\omega) \\ \hat{u}_2(\omega) \\ \vdots \\ \hat{u}_N(\omega) \end{pmatrix} = \sum_{n=1}^{4} \begin{pmatrix} h_n \exp(i\omega s_n z_1) \\ h_n \exp(i\omega s_n z_2) \\ \vdots \\ h_n \exp(i\omega s_n z_N) \end{pmatrix} u_n(\omega)$$

where

$\hat{u}(\omega)$ - the frequency spectrum for three-component data,
h_n - the unit polarization direction vector of the nth waveform,
s_n - the apparent slowness of the nth waveform,
$u_n(\omega)$ - the frequency component of the nth waveform.

The unit polarization direction vector is defined by incident angles θn

$$h_n = \begin{pmatrix} \sin\theta_n \\ \pm\cos\theta_n \end{pmatrix}$$

for compressional waves, and

$$h_n = \begin{pmatrix} -\cos\theta_n \\ \pm\sin\theta_n \end{pmatrix}$$

for in-plane polarized shear waves (SV) with + and - indicating downgoing and upcoming waves, respectively.

Usually it can be assumed that downgoing compressional and shear waves, and upcoming compressional and shear waves are locally superimposed as plane waves at a large propagation distance. The parameters of the polarization angle, the apparent slowness, and the frequency spectrum of the nth waveform are determined by minimizing the mean squared error between the model and the observed data.

$$E = \sum_{\varpi} \sum_{n=1}^{N} \left\| \hat{u}_k(\omega) - u_n(\omega) \right\|^2$$

The nonlinear parameters of the polarization angles and the apparent slowness are estimated by a nonlinear least square estimation for the Rosenbrock function (Esmersoy, 1988; Leaney and Esmersoy, 1989; Esmersoy, 1990). The inversion problem is overdetermined by taking frequency samples under the condition of more than two depth levels for inversion.

Inversion results

An initial model of the inversion was constructed by coarsely picked, apparent traveltime readings from the zero-offset VSPs in the shallower depth range, and from velocities calculated by seismic velocity analysis below the total depth of the well. By repeating the inversions, it turned out that the final inversion results were not strictly dependent on the initial model selection. Final velocity inversion was conducted over five traces at each depth level. In general, increasing the number of traces decreased the resolution of the inversion.

The velocity data derived by the inversion is shown in Figures 3 and 4 for compressional-wave and shear-wave velocities, respectively. Figure 5 illustrates the extracted wavefield. For comparison purposes, the compressional-wave and shear-wave velocities derived by DSI measurement are overlaid on these figures, not including the cased-hole DSI measurement of the shear waves. The compressional-wave velocity of the offset VSP is consistent with that of the zero-offset VSP estimated by the first-break picking. This means that the compressional-wave velocity field is laterally homogeneous in the current, rather smaller, offset geometry between the source and the receiver. Some doubtful velocity values were estimated using the inversion, but it is clear that

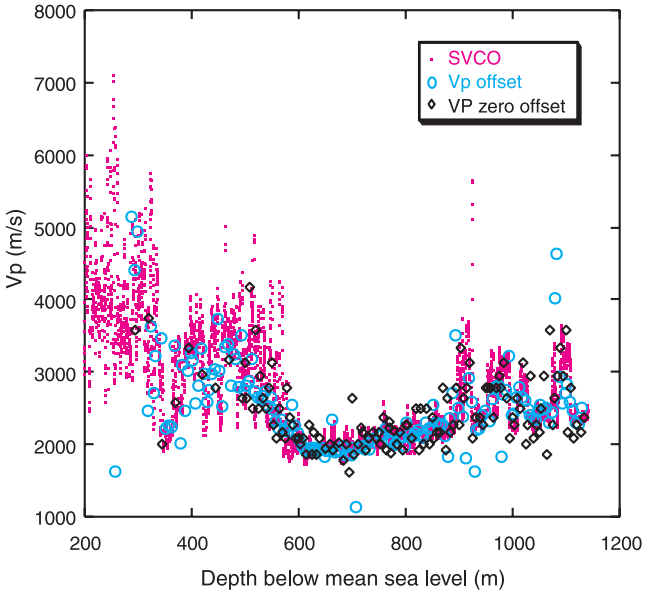

Figure 3. *Compressional-wave velocities (Vp) estimated by wavefield inversion method for offset VSP, traveltime inversion for zero-offset VSP, and monopole DSI sonic velocities.*

the general trend of estimated velocities is consistent with the compressional-wave velocity estimated using the DSI tool over almost all depths.

For the inversion of shear waves in the depth interval between approximately 650 and 840 m, estimated shear-wave velocities show values smaller than the shear-wave velocities estimated by STC processing of DSI data. The discrepancy between estimated shear-wave velocities using the inversion method and the DSI shear-wave velocity trend is consistent with the discrepancy between the traveltime reading of the zero-offset VSP and DSI shear-wave velocity trend (Sakai, 1998). By these independent estimates, it can be concluded that shear-wave velocities estimated by DSI measurements show greater velocity estimates than those of VSP data. The missing or unreliable data acquired in the second run of DSI measurement in the cased hole can be filled in by the inversion result or the traveltime analysis of VSP data.

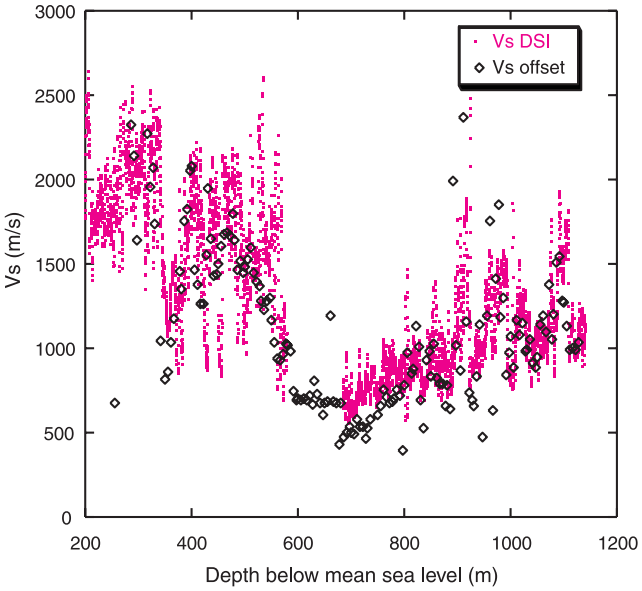

Figure 4. *Shear-wave velocities (Vs) estimated by wavefield inversion method for offset VSP and DSI sonic velocities.*

GENERATION OF SYNTHETIC SEISMOGRAMS

Logging-data drift correction

Acoustic transit-time logs were corrected by analyzing drift values between VSP traveltimes and integrated acoustic transit times. Calibration points were selected and drift values were linearly interpolated between them. Averaged drift values for the compressional-wave transit-time log are relatively small and less than 4 µs/ft. But drift values for the shear-wave sonic log exceed 35 µs/ft in the depth range between 677 and 889 m and 33 µs/ft in the depth range between 338 and 571 m. As the data-quality problem remained for the DSI measurements in the cased-hole interval, drift values are assumed to be zero in shear-wave transit-time log. The datum of these traces was reduced to the mean sea level unless noted otherwise. It is interesting that the drift values remained positive for the whole depth interval except the zone assumed to be zero for both the compressional- and shear-wave transit-time

Table 3. Averaged drift-correction values for sonic transit-time log.

Shear wave slowness	
Depth below mean sea level (m)	**Averaged drift correction (µs/ft)**
92–338	0
338–571	33.18
571–677	0
669–889	35.13
889–1132	7.76
Compressional-wave slowness	
Depth below mean sea level (m)	**Averaged drift correction (µs/ft)**
93–563	3.37
563–668	0
669–889	0.69
889–1132	3.38

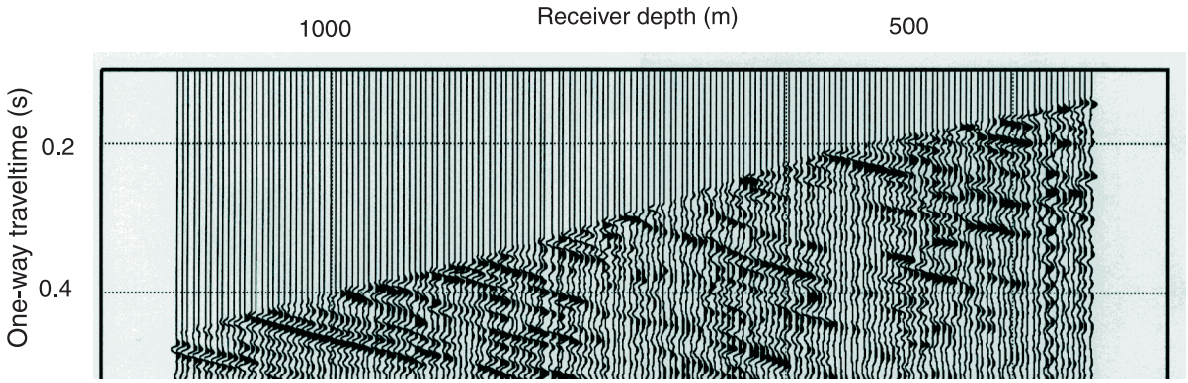

Figure 5. *Extracted compressional wavefield by the inversion method.*

logs. Logging data show greater velocity values than data in the seismic-frequency band. The averaged drift corrections are listed in Table 3.

The relations between the compressional wave and shear wave velocities are estimated by cross-plotting the logging data after drift correction with the VSP data.

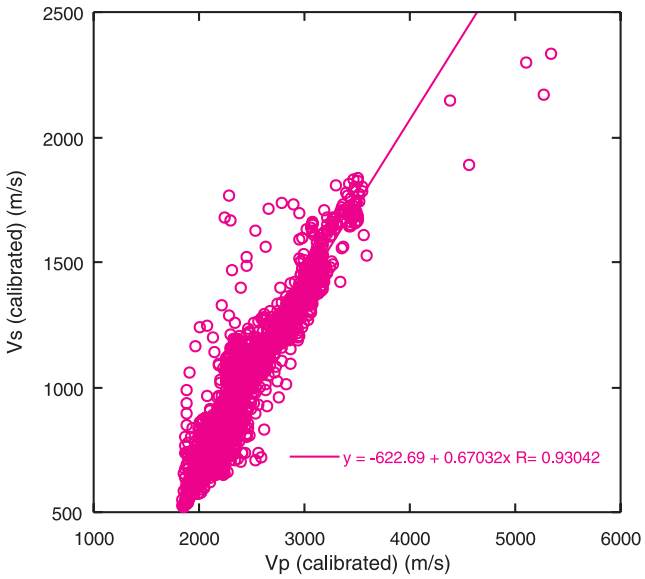

Figure 6. *Cross plot of the drift-corrected compressional- (Vp) and shear-wave (Vs) velocity from the 685–1150 m interval. A linear regression curve is fitted by the least-square method between both velocities.*

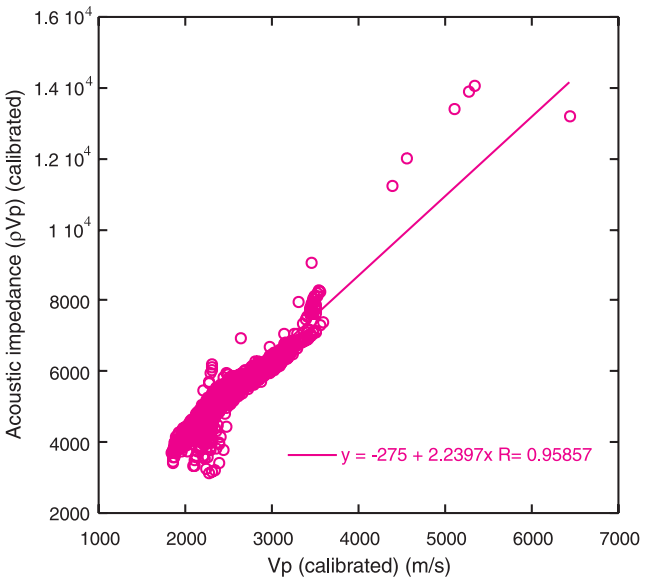

Figure 7. *Cross plot of the acoustic impedance of drift-corrected compressional-wave velocity (ρVp) and the drift-corrected compressional-wave velocity (Vp) for the 685–1150 m interval. A linear regression curve is fitted by the least-square method between both values.*

$V_S = -622.69 + 0.67032V_P$
V_P - compressional wave velocity in m/s
V_S - shear-wave velocity in m/s

In the depth interval 685–1150 m below KB, a linear curve fitting gives good correlation with a correlation coefficient 0.93042. It is shown in Figure 6.

Also in the depth interval between 685 and 1150 m below KB, the acoustic impedances and the compressional- and shear-wave velocities after drift correction by VSP data are linearly correlated with correlation coefficients 0.95857 and 0.98414, respectively (Fig. 7 and 8).

$\rho Vp = -275 + 2.2397V_P$
$\rho V_S = -66.61 + 2.1959V_S$
ρ - bulk density in g/cm^3

The measured bulk-density log shows truncated values in the permafrost zone, which implies the density is close to 1.0 g/cm^3 which could not used for quantitative analysis.

Synthetic seismograms

In the computation of synthetic seismograms for compressional and shear waves, bulk-density values were assumed to be 2.0 g/cm^3 in depths shallower than 678 m, where the density values are truncated in the bulk-density log measurements. For compressional-wave synthesis, the velocity and density logs were resampled at 1 ms two-way time, and using the resampled acoustic-impedance log, reflection coefficients were synthesized and filtered with a trapezoidal pass-band of 10, 12–175, and 200 Hz to correlate with zero-offset compressional-source-mode VSP data. For

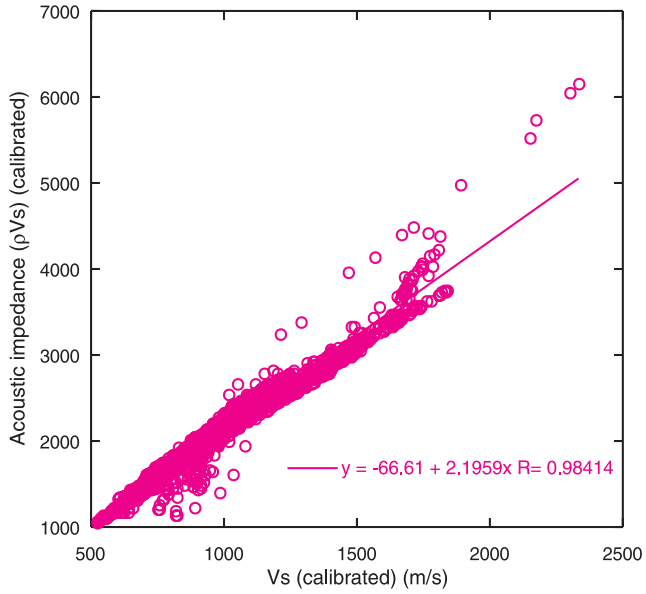

Figure 8. *Cross plot of the acoustic impedance of drift-corrected shear-wave velocity (ρVs) and the drift-corrected shear-wave velocity (Vs). A linear regression curve is fitted by the least-square method between both values.*

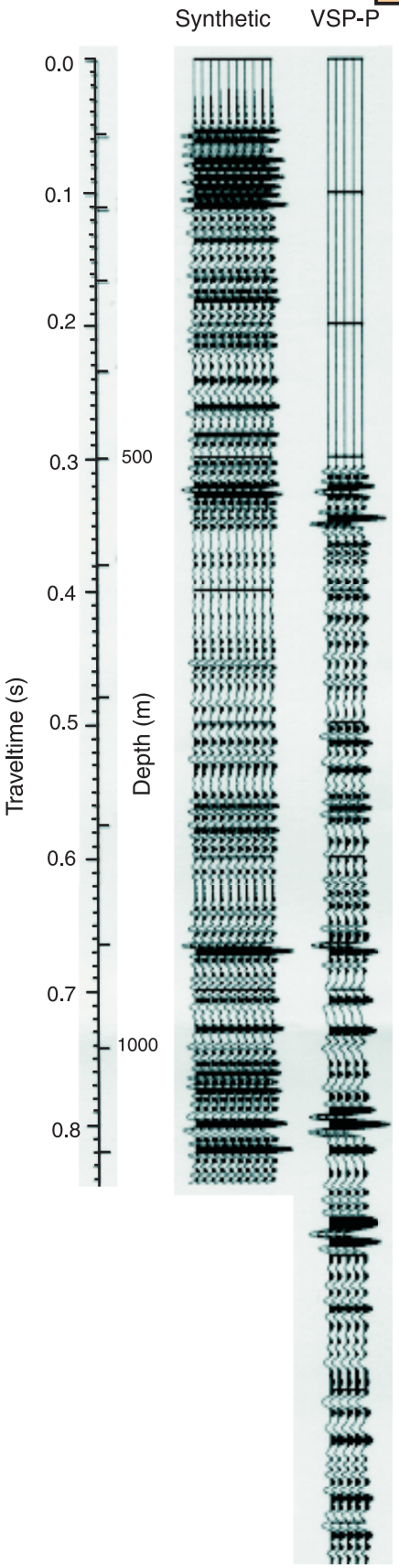

Figure 9. *Composite display of synthetic seismogram of drift-corrected compressional sonic velocity and compressional-source-mode zero-offset VSP stack section.*

shear-wave synthesis, the velocity and density logs were resampled at 1 ms two-way time, and using the resampled acoustic-impedance log, reflection coefficients were synthesized and filtered with a trapezoidal pass-band of 8, 12–40, and 60 Hz to correlate with zero-offset shear-source-mode VSP data.

Figures 9 and 10 illustrate the filtered synthetic seismogram and the final zero-offset VSP stacked section for compressional-source-mode and shear-source-mode VSP,

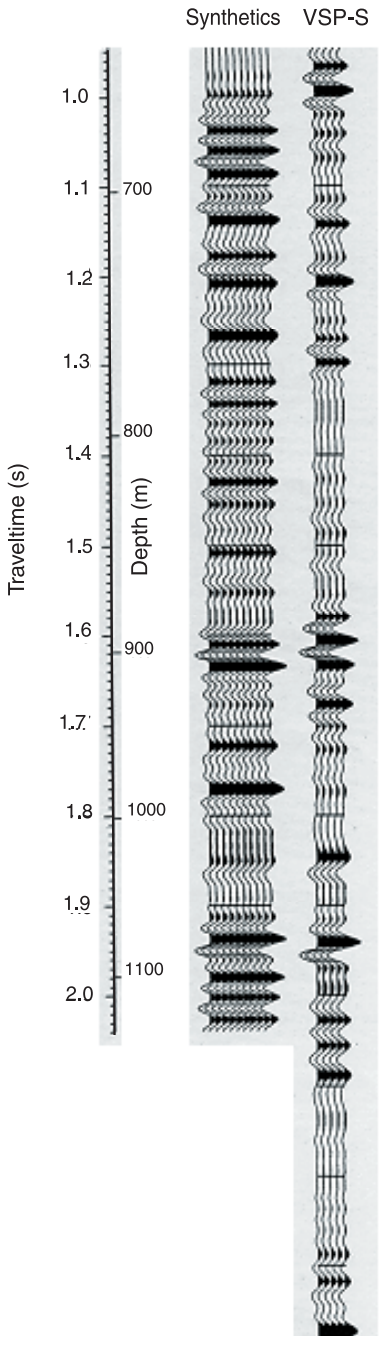

Figure 10. *Composite display of synthetic seismogram of drift-corrected shear sonic velocity and shear-source-mode zero-offset VSP stack section.*

respectively. The correlation between the two sets of traces is excellent, especially for the compressional-wave-mode VSP, which fully justifies the processing scheme of the log-data drift correction and VSP data. In the seismic-frequency range, drift-corrected wireline data and VSP data showed almost the same result. This means that the borehole effects, such as filtrate invasions, etc., were not serious or did not exist at the acquisition stage for conventional wireline data, as VSP data are essentially free from these effects. The VSP data provides good starting data for the evaluation of the spatial extent of the elastic parameters. For shear-wave zero-offset VSP data, the amplitudes of the synthetic seismogram and the VSP stacked section are inconsistent. One of the reasons is that bad traces were removed before stacking and the amplitude of the VSP section is not fully balanced in the whole section. The weak reflection zone between 780 and 850 m in the VSP section corresponds to the zone where the shear particle motion of the first break departs from a linear-polarization pattern. Therefore, shear-wave mode contamination by anisotropy effects causing such departure from a linear pattern may be related to the apparent amplitude decay in this interval. Between 950 and 1000 m, an amplitude-inconsistent zone exists where there is no striking departure from linear polarization and the shear-wave mode is well separated in the processing. The amplitude may be highly attenuated, as the velocity contrast is relatively large in this interval.

Using the calibrated compressional-wave transit-time log, root mean square (RMS) velocity can be computed and compared with the results of the seismic-velocity analysis. The Mallik 2L-38 well is located on the surface seismic line 82028 which was acquired in 1977 by Imperial Oil Limited. These data were reprocessed and the stacking velocities in the area of the well were estimated. Figure 11 illustrates the RMS velocity computed by the calibrated compressional-wave

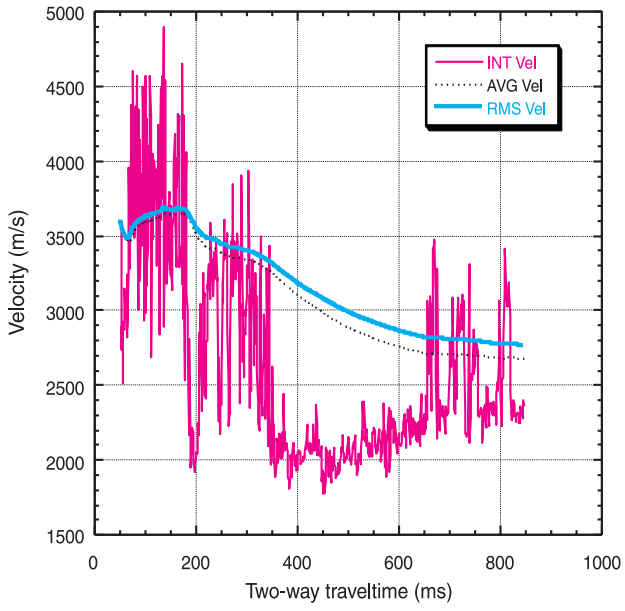

Figure 11. *Drift-corrected compressional sonic velocity log (INT Vel), average velocity (AVG Vel), and root mean square velocity (RMS Vel) as a function of two-way traveltime.*

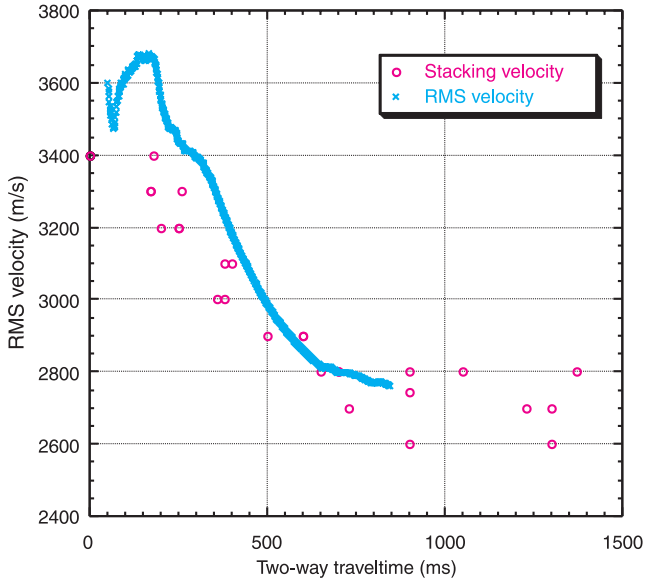

Figure 12. *Stacking velocity of line 82028 at Mallik 2L-38 and root mean square velocity of drift-corrected compressional sonic velocity log as a function of two-way traveltime.*

transit-time log and Figure 12 illustrates the estimated stacking velocities at CMP (common midpoint) locations close to the well on line 82028. In the permafrost zone shallower than 0.4 seconds two-way time, the stacking velocities are smaller than the log-derived RMS velocity. The near-surface velocities were assumed and not directly estimated in the seismic processing itself as the standard weathering-velocity analysis method could not be applied in the permafrost area. For the log-derived RMS velocity, the uppermost compressional-wave velocity is extrapolated from around 100 m. According to the seismic-velocity trend below 0.85 s, the velocity gradient becomes much gentle. The stacking velocity is approximated by the RMS velocity under the conditions that the ray-bending effects are negligible and the offset distance is small to satisfy the hyperbolic assumption. In this case, the condition is not fulfilled as the velocity largely decreases in the deeper zone and the ray bends divergently. This causes a higher stacking velocity than RMS velocity if all the traces were used. The problem is that the seismic-data quality is poor in the shallower zone. The error is partly related to the reversed velocity trend in permafrost areas where the prominent reverberations are enhanced in the shallower layers and hard to remove without muting the farther traces. Therefore, the errors existing in the velocity estimate are inconsistent with the RMS estimate.

POLARIZATION ANALYSIS

Linearity factor in the polarized wave motion

In the course of processing both shear-source-mode zero-offset VSP and compressional-source-mode offset VSP data, the polarization angles are estimated to transform the original

data recorded by a two- or three-component receiver into radially and transversely oriented data components. For the compressional-source mode, the polarization of the incident compressional wave of the first break is estimated by particle motion analysis. It is based on the eigenvector analysis of the covariance matrix under the assumption of Gaussian noises superimposed on the signal. The largest eigenvalue determines the major polarization direction. To examine the characteristics of the incident waves and to judge the efficiency of the separation method, the concept of a linearity factor is introduced. It is defined by the value that equals the ratio between the second principal eigenvalue and the maximum eigenvalue subtracted from one. If the linearity factor is close to one, the first-break motion is linearly polarized in the propagation direction. These values are computed in any two-dimensional planes, e.g. the horizontal plane, the plane constructed by the incident and transverse directions, and others. For shear-source-mode zero-offset VSP, the largest eigen direction in the horizontal plane is assumed to be the source direction. Note that the polarization analysis is not done for the compressional-source-mode zero-offset VSP, and the largest eigen direction is the vertical. It is difficult to use any horizontal components.

According to the investigation of Mallik 2L-38 data, the linearity factor was close to one and that indicates that the reorientation processing was executed satisfactorily. Above a depth of approximately 650 m, the linearity of the first-break motion was excellent and the uncertainty was extremely small for the transformation of the polarized waves into the well-defined directions. In the deeper zone, the depth intervals have different linearity factors, i.e. there are three or four different linearity-factor zones in the subsurface at depth. There appears to be no direct correlation of the linearity factor between the compressional- and shear-source modes. Degradation of the linearity factor in the compressional-wave data is partly related to the wave-mode conversion at the receiver points.

Indication of the anisotropy

Figure 13 illustrates the seismic record where, in the shear-source-mode zero-offset VSP, shear-wave first breaks are transformed into transverse and radial directions, and aligned with the same time origin. Figure 13 shows that the radial component is faster in the depth zone below approximately 680 m and slower in the depth zone above approximately 680 m than the transverse component, measuring approximately 25 ms and 0–50 ms respectively. This would be an indication of anisotropy related to the source-polarization direction. The nature of the anisotropy is different in the two depth zones. In the deeper zone (annotated as zone II) the first break of the shear wave in the radial component is faster. In the shallower zone (annotated as zone I) the two perpendicular shear-wave first breaks have the same time difference.

One model of anisotropy is based on the horizontal stress and fracture orientation. The polarization direction of the faster shear wave is close to the direction of the fracture and to the maximum horizontal compressional stress. The fracture orientation in zone I would be close to the direction of the initial shear-wave source motion. In zone II it would be close to the perpendicular direction of the initial shear-wave source motion. As, in practice, the VSP survey was not conducted with fully polarized source orientations, the following discussion remains speculative. Below the bottom of the permafrost, the depth of which is hard to determine by the wireline data alone if it occurs within the cased hole interval, there seems to be a change in fracture orientation that is close to perpendicular to the fracture orientation in the permafrost.

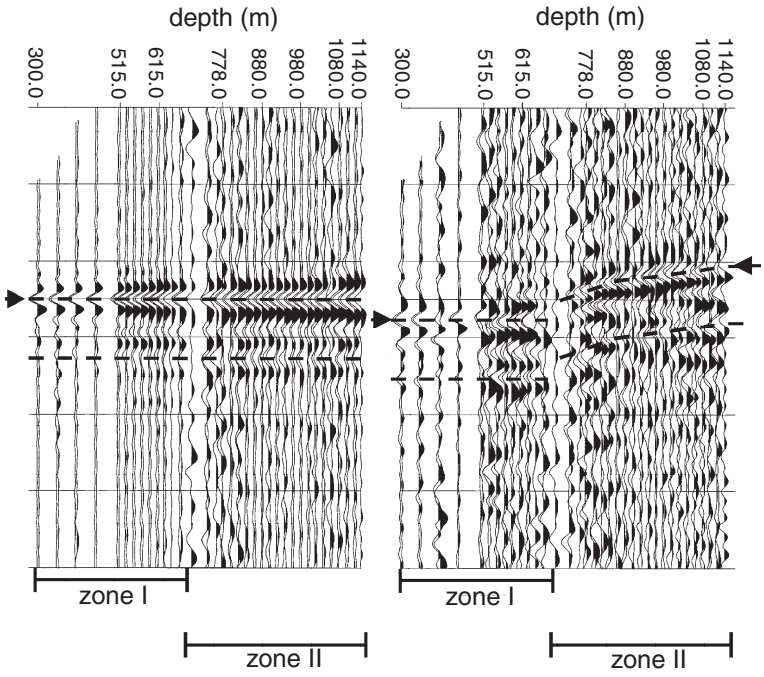

Figure 13.

VSP records of shear-source mode that illustrate the indication of anisotropy of different modes in zone I and zone II. The record on the left is the transversely polarized horizontal component and the record on the right is the radially polarized horizontal component.

The fracture direction of the shallower zone I is almost perpendicular to the direction connecting the Mallik L-38 and new Mallik 2L-38 wells in the shallowest zone, while in the deeper zone II it is closer to the connecting direction between the two wells (*see* Fig. 1). As this polarized velocity is faster in zone II, the density of fracture may be greater in the deeper zone. The fracture orientation is related to the fault patterns in these areas, which shall be discussed based on the surface seismic data.

The shallower part of zone II corresponds to the zone where the shear-wave velocity estimated by DSI is faster than the shear-wave velocity estimated by VSP. The direction of the incident ray is almost vertical and the direction of the ray propagation of DSI is also vertical. But the DSI was operated only under the upper-dipole mode and the source polarization was not constrained. Therefore, there is a lack of DSI data for discussing anisotropy. It is probable that the macro-fractures have a different orientation from the log scale. For detailed fracture-orientation analysis, DSI should be operated under crossed-dipole mode with in-line and crossed-line 32-receiver configuration.

SURFACE SEISMIC DATA

Stratigraphic inversion of seismic data

Seismic data reprocessing

Seismic data from line 82028 (*see* Fig. 1) and others were reprocessed to generate an impedance (or velocity) log calibrated at the location of Mallik 2L-38. A seismic-data velocity log was generated from the drift-corrected compressional- and shear-wave velocity logs. Several methods were examined to enhance the data quality. The main objectives of the reprocessing were to enhance the resolution and to estimate a more reliable seismic velocity.

The recording parameters for the seismic survey are summarized in Table 4.

Stratigraphic inversion

Stratigraphic inversion is a method used to estimate velocity structure by means of poststack seismic data combined with logging data. A classical problem in the geophysical research community is how to rationally generate velocity logs, and there are many known approaches to inversion. Recently, it was highlighted as one of the reservoir characterization techniques in the industry.

Table 4. Seismic survey specifications.

Instrument	TI DFSV
Record length	7 sec
Sampling rate	2 msec
Recording filter	12–124Hz
Source	Dynamite
Shot interval	400 ft
Shot depth	62–120 ft
Charge size	75 lbs
Geophone	14 Hz Mark-L10
Group interval	100 ft
No. of group	96
Spread geometry	Split-spread

This inversion is based on the model of convolution of the zero-phase wavelet and the reflection-coefficient series with additive noise. The recursive method integrates the original impedance series and produces the higher frequency component of the impedance series. The lower frequency component is supplemented by the velocity log data from the well. The method of model-based inversion starts with the initial model and changes the model iteratively to minimize the least squared error.

In the inversion of the current data to estimate acoustic impedance, the model-based method is applied by using velocity log data as an initial model. The relation between acoustic impedance and velocity, which was derived from the cross plot, is used to transform the acoustic impedance into the velocity.

Figure 14 illustrates an example of a velocity log estimated by using the seismic traces based on the blocking inversion method. The layer where the gas hydrate cores were recovered extends laterally in this velocity section if the higher velocity is taken as a marker. There is a discrepancy in the velocity values derived from well-log data and seismic-log data at the well. The main drawback is that the dominant frequency of the seismic traces is less than 70 Hz. This is related to low seismic resolution and neighbouring velocity peaks which have not been well separated by the inversion methods.

Stratigraphic data

A significant velocity change exists at a depth of around 560 m in the permafrost zone. Below approximately 560 m, the velocities increase linearly. This velocity change is shown clearly on the VSP processed section and the inversion section of line 82028 as a higher velocity reflector at about 0.35 s two-way traveltime. This higher velocity zone ends at the Mallik 2L-38 well and extends to the east. The terminated reflector is interpreted to be on the hanging-wall side of a normal fault along the flank of the Mallik anticline.

The lithostratigraphy of Mallik 2L-38 has been assessed mainly by using the lithostratigraphic data provided by Jenner et al. (1998):

Iperk Sequence: 0–346 m below KB
Mackenzie Bay Sequence: 346–926.5 m below KB

These boundaries do not correspond to velocity boundaries and some are in the reflection-free zone.

It is important to note that there is a change of the estimated depth of stratigraphic boundaries between both wells. Unless there is some biostratigraphic interpretation allowance to account for the change, the other possible explanation is that the reflector termination stated above may be related to the interpreted normal faulting.

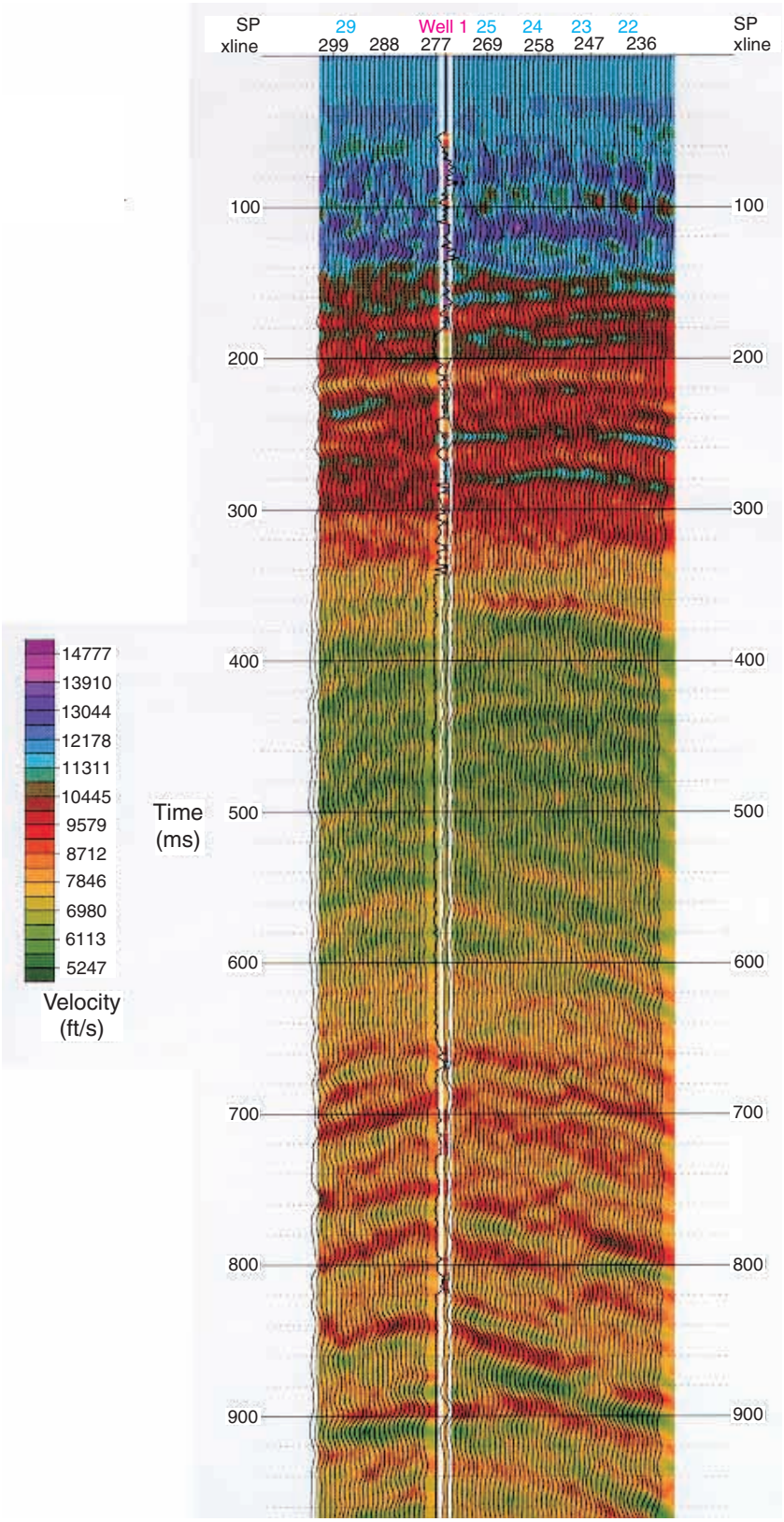

Figure 14.

Velocity log of line 82028 calibrated at Mallik 2L-38 and estimated by the stratigraphic-inversion method.

It is difficult to identify the base of the permafrost zone using only the velocity data from around 638.7 m (the depth of permafrost predicted from the Mallik L-38 well data). According to the data discussed previously in this paper dealing with the polarization analysis, the boundary exists at approximately 680 m, characterized by the change in the anisotropy mode. The change in the anisotropy was explained by the change in the fracture orientation, which was related to the existence of a normal fault close to the well. One thing to be taken into account is that if the tectonism is governed by the normal or listric faulting, as evidenced by regional geology in the area, the maximum compressional stress is not on the horizontal plane as presumed in the preceding discussion. In that case, the fractures are obliquely oriented to the vertical direction and the overburden pressure contributes further to the actual fracture orientation. Fault direction is determined by the regional stress orientation and the frictional angle. If the frictional angle is assumed constant, the change in fracture orientation reflects the change in regional stress and the change in the fault-plane orientation. Such changes of the fault plane orientation might occur in zone II. Listric fault movement may cause a stress orientation change if the fracture orientation changes to the vertical in the deeper section and contributes to the increase in anisotropy.

ESTIMATE OF THE GAS HYDRATE QUANTITY BASED ON ROCK PHYSICAL MODELS

Gas hydrate was sampled in the sandy sediments and the maximum pore saturation of the gas hydrate exceeds 70%. To account for the seismic velocity in the gas-hydrate-bearing zone, rock physical models are examined. Average porosity is 0.3–0.35 for gas-hydrate-saturated layers, and quartz is the main constituent in the solid phase. The other constituent in the solid phase is clay, but the percentage is very small in the gas hydrate-bearing interval. As a first approximation, the gas-hydrate-bearing zone can be modelled as 100% quartz with 30% bulk porosity. Gas hydrate was disseminated homogeneously in the pore space according to observations of the sampled core where no massive or nodule-type gas hydrate was recovered. In addition to the calibrated compressional- and shear-wave velocity from this study, the logging data from conventional wireline surveys were also used to estimate porosity, water saturation, and mineral composition based on the neutron-density cross-plot method, Archie's relation for resistivity logs, and other methods (Miyairi et al., 1998). Density and solid-frame elastic bulk moduli were recomputed taking into account the estimated mineral composition.

The objective of this section is to evaluate the two opposing gas-hydrate-bearing models, that are tentatively called the 'compaction model' and the 'cementation model' and to compare the calibrated log velocities with the computed velocities. These models characterize the distribution of gas hydrate in the pore space and determine the seismic velocity as a function of gas hydrate saturation with other parameters.

Base velocity line computation — fully water saturated case

The base velocity line, defined as the velocity of fully water-saturated rock, was first computed based on what is called the 'Hashin-Shtrikman-Hertz-Mindlin model'. This is a bounding model (BM) connecting the point of zero porosity where the elastic moduli are those of the solid phase and the other point of critical porosity where unconsolidated rock is modelled by a random packing of identical elastic spheres. At the critical porosity, the effective bulk and shear moduli of the rock are computed by the Hertz-Mindlin theory (Mindlin, 1949). The two points are connected with the lower Hashin-Shtrikman boundary by porosity normalized by the critical porosity (Hashin and Shtrikman, 1963; Dvorkin and Nur, 1996). The lower and upper Hashin-Shtrikman boundaries are illustrated by the elementary model of spherical shell of the mixture constituents. As proposed by the initial model, below the critical porosity, two points are connected. One is the critical porosity point and the other is the zero porosity or void point. Two points are connected with the upper Hashin-Shtrikman boundary by partitioning the concentration of the void- and sphere-packed critical phase (J. Dvorkin and A. Sakai, unpub. rept., 1997). The major point of the model modification is how the suspended or pore-water-supported grain state is properly simulated below critical porosity as compared with measured finite rigidity.

The elastic moduli of the mixture of solid minerals were computed by the Hill average of each constituent of the mixture, which is the arithmetic average of Reuss average and Voigt average (Hill, 1952). For rock saturated with pore fluid, the shear modulus is assumed to be the same as that of the dry rock and the bulk modulus is computed by the Gassmann equation (Gassmann, 1951). The Gassmann equation simulates the elastic behaviour of the fluid-saturated rock in the seismic frequency bands except in the case of an extremely small pore aspect ratio, such as a fracture.

Elastic velocity of gas-hydrate-saturated rock

Dissemination (or compaction) model

The first model is the modification of the fully water saturated model. There are two cases for this model. One is the model where the gas hydrate is suspended in the pore fluid. The other model is where the gas hydrate constitutes part of the solid frame. For the first case, pore-fluid bulk moduli are modified by the Reuss average with the gas hydrate bulk modulus taken into account. If the gas hydrate constitutes part of solid frame, the porosity is reduced and solid-bulk and shear moduli are modified by the Hill average. The velocity calculated by the latter model shows a higher velocity than that calculated by the former. The gas hydrate 'compaction model' is analogous to compaction in the sense that pore space is simply reduced from an unconsolidated state where no cementation is assumed.

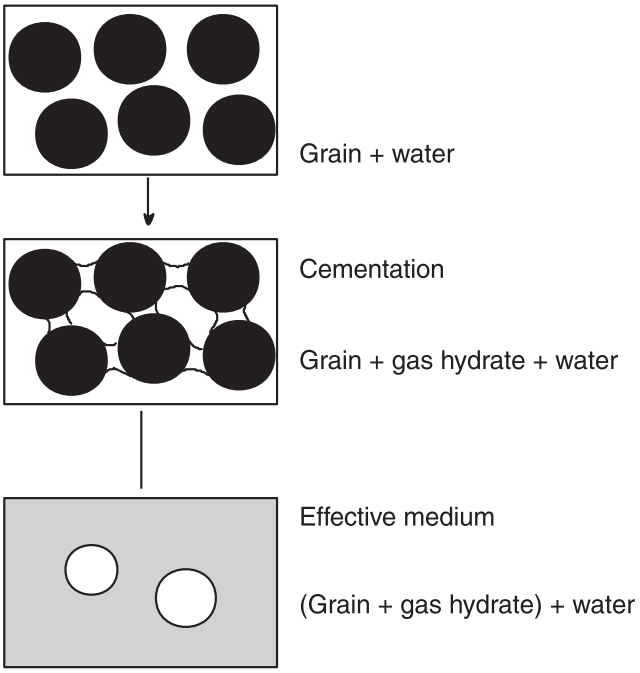

Figure 15. *Example of the cementation model using the self-consistent method (SCM) for higher gas hydrate saturation.*

Inclusion and cementation model

Rock saturated by large amounts of gas hydrate is modelled by gas hydrate inclusion in the fully water-saturated matrix. There are several modifications to the model. One approach is to take fully water-saturated rock as 'matrix' with fully gas-hydrate-saturated 'inclusions' distributed in the 'matrix'. If there are no data regarding the shape of the inclusions, they may be assumed to be spherical or ellipsoid. In practice, the inclusions may be less than fully saturated with gas hydrate. Then the saturation rate in the 'gas hydrate inclusion' can be considered as one of the controlling parameters. Observations of the sampled core showed no such fully saturated gas hydrate inclusions were measured at the macroscopic scale. The inclusion and cementation model was examined expecting, possibly in the larger scale, there might be mega-scaled inclusions.

The proposed inclusion and cementation model was analyzed using effective-medium theories (Wu, 1966; Berryman, 1980). As an example, the self-consistent method (SCM) is used for estimating the effective elastic moduli for the composite of three constituents (i.e. matrix, cement, and void). By introducing the effective medium constituting the cement at the contact point in the neighbourhood of the critical porosity, and assuming that there is no cementation in the void, the effective elastic moduli is computed using governing equations of SCM simulating the void as a sphere (Fig. 15). The empty void is then filled by gas hydrate and the elastic moduli of the void become those of gas hydrate. Finally the void is reintroduced into the 'matrix' and the elastic moduli are estimated as a function of the void or porosity (J. Dvorkin and A. Sakai, unpub. rept., 1997).

Computations

For the evaluation of models, the computations were first completed under the assumption of constant porosity, a solid frame of quartz grains, and a recomputed density sampled at 0.5 m and averaged over 5 points. Effective pressure was calculated from the recomputed density and an assumed brine density of 1.02 g/cm^3. Temperature and salinity effects for these parameters were not assumed, as the effects are small. In order to explain the measured density increase, the matrix density was estimated to be greater in the clay-rich intervals. If such density increases in the matrix frame are not taken into account, the computed solid-frame density calculated for solid components is decreased in the clay-rich interval. For the first estimate, the solid frame was assumed to be composed primarily of quartz. For the second estimate the recomputed density and solid-frame elastic moduli was used without assuming any density variation for each constituent in the solid phase. For simplicity, pore space was considered to be filled with water and gas hydrate. The contribution of free gas was not taken into account, as no major gas indication was observed in the well-log data.

Inclusion and cementation model

Figures 16 and 17 illustrate an example of computations based on the cementation model in the depth interval 850–930 m where evidence of accumulated gas hydrate was found in recovered core. Porosity was assumed to be constant and solid frame was assumed to be composed of quartz grains. Figure 16 shows the velocities at the assumed porosities of 0.2, 0.3, and 0.4 for the gas-hydrate-free state, and Figure 17 shows

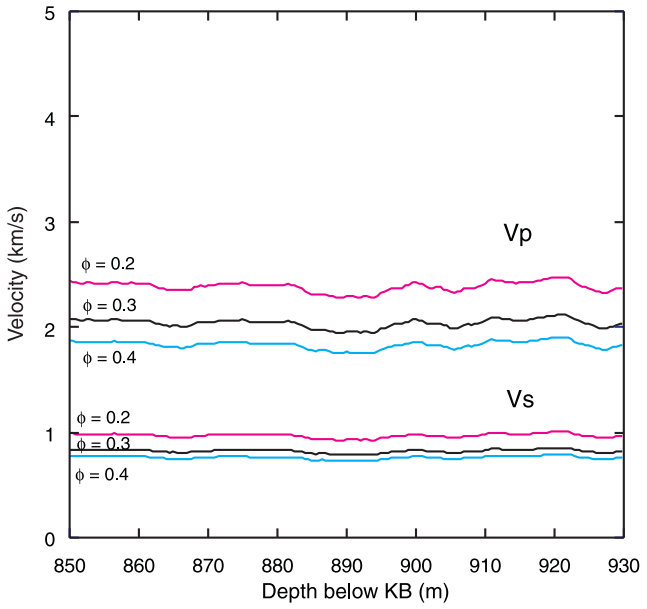

Figure 16. *Elastic-velocity computation for porosity values (ϕ) of 0.2, 0.3, and 0.4 under the gas-hydrate-free condition for the cementation model. Vp - compressional velocity, Vs - shear velocity.*

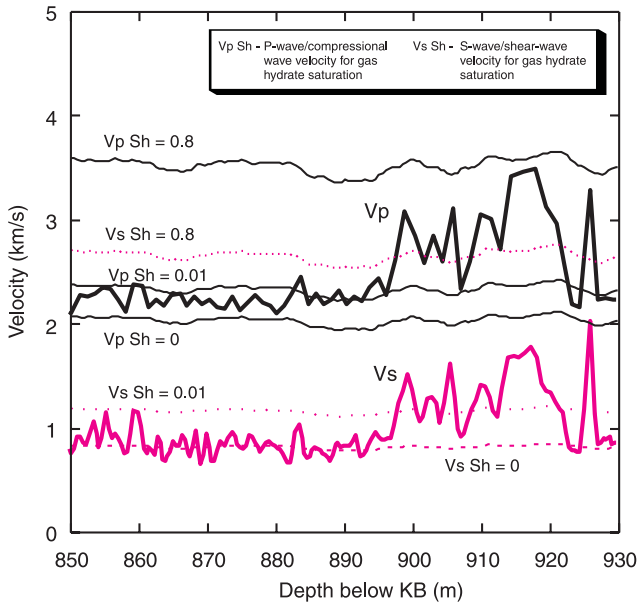

Figure 17. *Elastic-velocity computation for gas hydrate saturation values of 0, 0.01, and 0.8 in pore space with a porosity of 0.3 for the cementation model.*

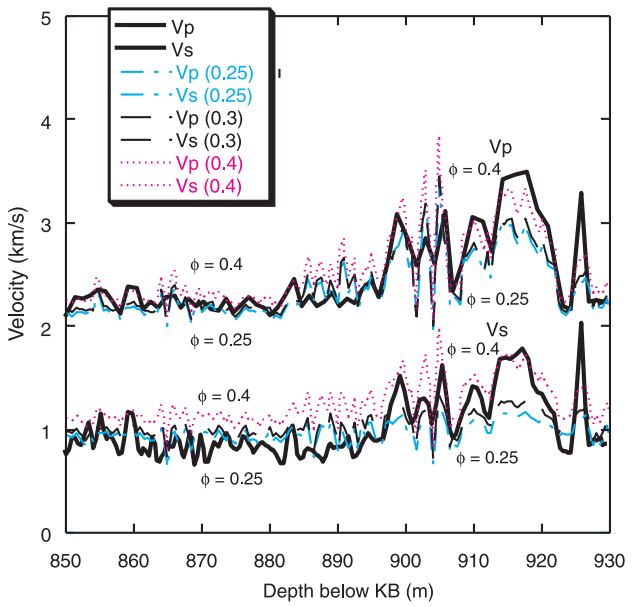

Figure 18. *Elastic-velocity computation for critical porosity values (ϕ) of 0.25, 0.3, and 0.4 under the estimated porosity and gas hydrate saturation by the neutron-density method and Archie's relation for the compaction model. Vp - compressional velocity, Vs - shear velocity.*

the velocities at gas hydrate saturations of 0.01 and 0.8 for porosity 0.3 overlaid on the calibrated compressional- and shear-wave velocities.

Without considering the actual variations in mineralogy and porosity in the depth interval, it is obvious from these figures that the cementation model does not simulate the observed shear-wave velocity though the base velocity line, showing that the gas-hydrate-free state looks reasonable. Within the selected gas hydrate saturation parameters, the compressional-wave velocities are within the allowable velocity range. Therefore, the shear-wave velocity is important for fixing the models. Very few reliable shear-wave velocities have been obtained from other gas-hydrate-related drilling projects. Any empirical time-average relations (Wood, 1941; Wyllie et al., 1958; Raymer et al., 1980; Pearson et al., 1983; Lee et al., 1993) use the compressional-wave velocity and essentially do not use shear-wave velocity for the rock constituent estimation. In Lee et al. (1996), the shear-wave velocity was incorporated into the relation of the compressional-wave velocity and empirically determined V_P/V_S combined with modified time-average relations.

Current computations based on models of sediment microstructure provide shear-wave velocity as well as compressional-wave velocity without assuming any empirical relations. According to the computations, there are uncertainties for the estimate of gas hydrate saturation only when using observed compressional-wave velocity.

Dissemination or compaction model

Figure 18 illustrates the computed velocities based on the compaction model. Elastic moduli are computed under an estimated mineralogy of quartz, clay, calcite, and coal. In the gas-hydrate-bearing interval, the quartz percentage is almost 100% in solid phase. The porosity and computed solid density from the mineral composition are averaged over 2.5 m. The parameters for each mineral are listed in Table 5. Thin coal layers were also identified, but in this study their contribution to the velocity distribution is negligible.

Table 5. Physical parameters of minerals in computation.

	Density (g/cm^3)	Bulk modulus (GPa)	Rigidity (GPa)
Quartz	2.65	36	45
Clay	2.58	20.9	6.85
Calcite	2.71	76.8	32
Gas hydrate	0.91	5.6	2.4
Water	1.02	2.29	0

In these computations, the critical porosity is considered a controlling parameter. The critical porosity is defined as the transition porosity between the solid-supported state and pore-water-supported state in water-saturated sphere packs. Random packing of identical spheres determines the number of contact points (Murphy, 1982). In marine sediments, it would not be unreasonable to assume well sorted sand grains. If the grain sorting was not sufficient in some facies, the number of these contact points and critical porosity might be varied. There are no such experimental data of varied radius distribution of spheres for the estimate of critical porosity and the number of contact points, but the clay may contribute to variations in these parameters in addition to the variations of the elastic moduli in the solid phase. The clay percentage is

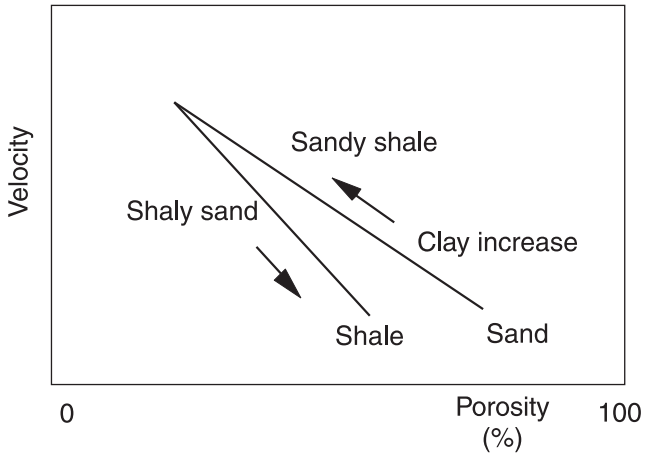

Figure 19. *A schematic velocity-porosity relation for a model of a sand-clay mixture with clay content as a parameter. This explains the contribution of clay content to critical porosity variations.*

estimated to be close to zero in the 910–930 m interval, and above 910 m clay percentage varied between approximately 5 and 65% in bulk volume.

The matches between computed velocities and observed velocities are better in the depth range below 910 m for a critical porosity of 0.4, and in the depth range above 910 m for a critical porosity of 0.25. The critical porosity variation in shear-wave velocity is more sensitive than in compressional-wave velocity. The critical porosity is a function of the sphere packing mode. The clay content increase is one parameter affecting it. The other would be the sphere-radius distribution in the layer.

Effect of clay in sand and gas hydrate mixture in compaction model

In sand and shaly sand, clay occurs in the sand pore space. In shale and sandy shale, clay is modelled as the matrix where sand grains are dispersed. When the clay-volume fraction is less than the pure sand porosity, clay particles locate in the sand pore space and the mixture porosity decreased linearly with increasing clay-volume fraction. When the clay-volume fraction becomes greater than the sand porosity, clay-particle addition makes the sand-grain lattice expand and the porosity of the mixture increases linearly with increasing clay content. When the clay-volume fraction equals the pure sand porosity, the porosity of the mixture reaches the minimum value, which is also evidenced by laboratory studies (Han et al., 1986). The relationship of velocity and clay content for a sand-clay mixture can be built by assuming proper bounding models. If the clay content is considered as a parameter, the velocity-porosity relationship is illustrated schematically in Figure 19. According to this schematic relation, the increase of clay content in the sand and gas hydrate mixture possibly decreases the critical porosity.

SUMMARY OF GAS HYDRATE MODELS

Elastic velocities were computed for two extreme models of gas hydrate-bearing sediments. In the cementation model, shear-wave velocity is very sensitive to the gas hydrate saturation, and the model will underestimate the gas hydrate saturation if an observed velocity is used for it. In the compaction model, both compressional- and shear-wave velocities closely match the estimated gas hydrate saturation. Therefore, the compaction model or the gas hydrate dissemination in pore space model better predicts the nature of the gas-hydrate-bearing sediments in the Mallik 2L-38 well. This model includes the parameter of inhomogeneous sphere-radius distribution in the rock. A simple binary model of a sand and shale mixture suggests that the contribution of the clay content to the critical porosity changes, but laboratory and field studies combined with microstructural consideration are needed to understand the ternary model of sand, clay, and gas hydrate in more detail.

CONCLUSIONS

In the Mallik 2L-38 gas hydrate research well in the Mackenzie Delta, Northwest Territories, Canada, a VSP survey with both shear- and compressional-source modes was conducted in order to integrate seismic data with geophysical logging and coring data. This was the first experimental survey related to gas hydrate quantification in a permafrost region. The VSP as a well-proximal seismic survey was successfully completed. The higher and broader seismic-frequency band compressional VSP survey fully supplemented the surface seismic survey, as partly evidenced by the comparison between stratigraphic inversion of surface seismic data and synthetic seismograms generated with calibrated velocities.

Traveltime-versus-depth relations were derived from compressional- and shear-source-mode zero-offset VSP surveys. According to the drift analysis of the traveltime between VSP and logging data, the drift of compressional-wave data was small. But the traveltime measured by the shear-source mode showed a larger delay than the integrated shear-wave transit-time log data in the depth interval from 677 m to 889 m. This may be explained by 1) velocity dispersion over frequencies, 2) anisotropy, 3) malfunctioning of tool or errors in the bias correction of the flexural-wave mode. The existence of anisotropy was suggested in VSP shear-source data, but a quantitative estimate was not reached, as the source was only arranged in the transverse direction.

Compressional- and shear-wave velocity was estimated for offset VSP data by the inversion technique simultaneously with the separation of wavefields. The compressional-wave velocity estimated by inversion shows good correlation with velocity estimated by zero-offset VSP traveltime analysis. The shear-wave velocity estimated by inversion was less than the shear-wave velocity estimated by DSI data in the interval of approximately 650–840 m, which is explained by the same

reasons for the drift in zero-offset VSP traveltime. Estimated velocity structures are consistent in data of both zero-offset and offset-VSP.

Two gas hydrate saturation models (i.e. cementation and compaction models) were examined which estimated gas hydrate saturation using resistivity logs. It was found that shear-wave velocity is the key data for fixing the model. Data showed that gas hydrate is disseminated in pore space with no prominent cementation at the grain boundaries.

ACKNOWLEDGMENTS

I would like to thank the Imperial Oil Resource Ltd. for providing surface seismic data in the Mallik 2L-38 area for our review and investigation. The operation of the VSP was financially supported by the Research Consortium of Methane Hydrate Exploration in Japan (JNOC, JAPEX and nine other organizations).

REFERENCES

Berryman, J.G.
1980: Long-wavelength propagation in composite elastic media; Journal of the Acoustical Society of America, v. 68, p.1809–1831.
Chen, S.T.
1988: Shear-wave logging with dipole sources; Geophysics, v. 53, p. 659–667.
Dankbaar, J.W.M.
1987: Vertical Seismic Profiling - separation of P- and S-waves; Geophysical Prospecting, v. 35, p. 803–814.
Devaney, A.J. and Oristaglio, M.L.
1986: A plane wave decomposition for elastic wave-fields applied to the separation of P- and S-waves in a seismic vector; Geophysics, v. 51, p. 419–423.
Dvorkin, J. and Nur, A.
1996: Elasticity of high-porosity sandstones: theory for two North Sea datasets; Geophysics, v. 59, p. 428–438.
Esmersoy, C.
1988: Velocity estimation from offset VSPs using direct P and converted SV waves; *in* Expanded Abstracts of 1988 Annual Meeting of the Society of Exploration Geophysicists, Society of Exploration Geophysicists, p. 538–541.
1990: Inversion of P and SV waves from multicomponent offset vertical seismic profiles; Geophysics, v. 55, p.39–50.
Everhart, A.H. and Chang, S.K.
1985: A theoretical study of dipole shear logging in cased hole; *in* Expanded Abstracts of 1985 Annual Meeting of the Society of Exploration Geophysicists, Society of Exploration Geophysicists, p. 72–74.
Gassmann, F.
1951: Uber die Elastizitat poroser Medien; Vierteljahreszeitschrift der Naturforschenden Gesellschaft in Zurich, v. 96, p.1–23.
Han, D., Nur, A., and Morgan, D.
1986: Effect of porosity and clay content on wave velocity in sandstones; Geophysics, v. 51, p. 2093–2107.
Hashin, Z. and Shtrikman, S.
1963: A variational approach to the elastic behavior of multiphase materials; Journal of Mechanical Physics and Solids, v. 11, p. 127–140.
Hill, R.
1952: The elastic behavior of crystalline aggregate; Proceedings of the Physics Society of London, v. A65, p. 349–354.
Jenner, K.A., Dallimore, S.R., Nixon, F.M., Winters, W.J., and Uchida, T.
1998: Sedimentology of methane hydrate host strataform JAPEX/JNOC/GSC Mallik 2L-38; *in* Proceedings of the International Symposium on Methane Hydrates: Resources in the Near Future?, Japan National Oil Corporation – Technical Research Center, Chiba City, Japan, p. 319–376.
Kurkjian, A.L.
1986: Theoretical far-field radiation from a low-frequency horizontal acoustic point force in a vertical borehole; Geophysics, v. 51, p. 930–939.
Kurkjian, A.L. and Chang, S-K.
1986: Acoustic multipole sources in fluid-filled boreholes; Geophysics, v. 51, p. 148–163.
Leaney, W.S.
1990: Parametric wave-field decomposition and applications; *in* Expanded Abstracts of 1990 Annual Meeting of the Society of Exploration Geophysicists, Society of Exploration Geophysicists, p. 1097–1099.
Leaney, W.S. and Esmersoy, C.
1989: Parametric decomposition of offset VSP wave fields; *in* Expanded Abstracts of 1989 Annual Meeting of the Society of Exploration Geophysicists, Society of Exploration Geophysicists, p. 26–29.
Lee, M.W., Hutchinson, D.R., Collett, T.S., and Dillon, W.P.
1996: Seismic velocities for hydrate-bearing sediments using weighted equation, Journal of Geophysical Research, v. 101, p. 20 347–20 358.
Lee, M.W., Hutchison, D.R., Dillon, W.P., Miller, J.J., Agena, W.F., and Swift, B.A.
1993: Method of estimating gas hydrates in deep marine sediments; Marine and Petroleum Geology, v. 10, p. 493–506.
Mindlin, R.D.
1949: Compliance of elastic bodies in contact; Journal of Applied Mechanics., v. 16, p. 259–268.
Miyairi, M., Akahisa, K., and Uchida, T.
1998: Well log evaluation techniques for natural gas hydrate bearing formation; *in* Proceedings of the International Symposium of Methane Hydrates: Resources in the Near Future?, Japan National Oil Corporation – Technical Research Center, Chiba City, Japan, p. 333–347.
Murphy, W.F. III
1982: Effects of microstructure and pore fluids on the acoustic properties of granular sedimentary materials; Ph.D. thesis, Stanford University, Stanford, California, 269 p.
Pearson, C.F., Halleck, P.M., McGulre, P.L., Hermes, R., and Mathews, M.
1983: Natural gas hydrate, a review of in situ properties; Journal of Physical Chemistry, v. 87, p. 4180–4185.
Randall, C.J., Scheibner, D.J., and Wu, P.T.
1991: Multiple borehole acoustic waveforms: synthetic logs with beds and borehole washouts; Geophysics, v. 56, p. 1757–1769.
Raymer, L.L., Hunt, E.R., and Gardener, J.S.
1980: An improvement sonic transit time-to-porosity transform, Transactions of the Society of Well Log Analysts, 21st Annual Logging Symposium, Society of Well Log Analysts, p. P1–P13.
Sakai, A.
1997: Seismic studies on marine gas hydrates offshore Japan; *in* Proceeding of the International Workshop on Gas Hydrate Studies at Tsukuba, Japan, Japan Science and Technology Agency, p. 222–229.
1998: Vertical seismic survey in the Mallik 2L-38 – specifications, data acquisitions and data analysis; *in* Proceedings of the International Symposium on Methane Hydrates: Resources in the Near Future?, Japan National Oil Corporation – Technical Research Center, Chiba City, Japan, p. 359–370.
Schmitt, D.P.
1988: Shear wave logging in elastic formations, Journal of the Acoustic Society of America, v. 84, p. 2215–2229.
Tjostheim, D.
1975: Autoregressive representation of seismic P-wave signals with an application to the problem of short-period discriminants; Geophysical Journal of the Royal Astronomical Society, v. 43, p. 269–291.
Wood, A.B.
1941: A text book of sound, Macmillan, New York, New York, 204 p.

Wu, T.T.
1966: The effect of inclusion shape on the elastic moduli of a two-phase material, International Journal of Solids and Structures, v. 2, p.1–8.
Wyllie, M.R.J., Gregory, A.R., and Gardner, G.H.F.
1958: An experimental investigation of factors affecting elastic wave velocities in porous media; Geophysics, v. 23, p. 459–493.
Yokota, T., Zhou, S., Mizoue, M., and Nakamura, I.
1981: An automatic measurement of arrival time of seismic waves and its application to an on-line processing system, Bulletin of the Earthquake Research Institute, v. 56, no. 3, p.449–484.